Correlating soil properties with post-yield oedometer stress-strain behavior of Finnish sensitive clays through $\text{PoYOSS}_{\text{Clay}}^{Sen}$

Mohammad Sadegh Farhadi [1*], and *Tim T.* Länsivaara [1]

[1] Research Center Terra, Department of Civil Engineering, Faculty of Built Environment, Tampere University, Tampere, Finland

Abstract. A novel post-yield oedometer stress-strain prediction model, $\text{PoYOSS}_{\text{Clay}}^{Sen}$, was developed at Tampere University, Finland, for Finnish sensitive clays. As a typical characteristic behavior of sensitive clays, in CRS oedometer tests, rapid deformation occurs immediately after yield stress. The post-yield phase can be approximated accurately by three parameters: a limit constrained modulus M_L, a limit stress interval for destructration phase S_L, and a modulus number M', proposed by Sällförs (1975). In one of the five principal submodels of $\text{PoYOSS}_{\text{Clay}}^{Sen}$, as the learning-based predictor, multi-layer perceptron (MLP) artificial neural network (ANN) was utilized to estimate M_L, M', and S_L. This study investigated the correlations between these three deformation parameters and various combinations of soil properties via the mentioned submodel. For this data-driven assessment, a database was employed comprising five Finnish testing sites of sensitive clays, with sensitivity ranging from 14 to 122. The analysis indicated which soil properties exhibited the strongest correlations with each of M_L, M', and S_L. In general terms, it was revealed that these three parameters were highly correlated with water content, w_n, fallcone shear strength for intact state, $S_{u,int}$, yield effective stress, σ'_y, and plastic limit, w_p.

1 Introduction

In consolidation theory, a very basic chart is the void ratio-effective stress behavior, often drawn in semi-logarithmic scale, as $\log(\sigma'_v) - e$. The logarithmic scale of σ'_v simplifies acquisition of two indices for the pre- and post-yield states, respectively, known as recompression index, C_r, and virgin compression index, C_c, as the slopes of the chart. The simplification to acquire indices in semilogarithmic scale is presented in Figs. 1(a-b).

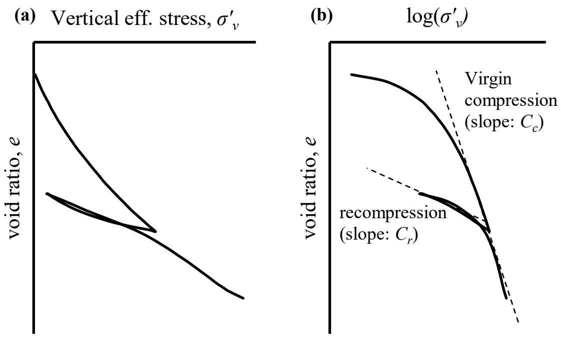

Fig. 1. Typical (a) deformation behavior chart (in linear scale), to find (b) virgin compression index, C_c, and recompression index, C_r (in semi-logarithmic scale).

Provided that C_c is known from experiments, deformation for the post-yield state can be calculated as the one-dimensional oedometer strain, ε_a, as:

$$\varepsilon_a = \frac{C_c}{1+e_0} log\left(\frac{\sigma'_1}{\sigma'_2}\right) \tag{1}$$

for any vertical effective stress interval $\Delta\sigma'_v = \sigma'_1 - \sigma'_2$. The parameter e_0 represents initial void ratio.

There are numerous studies providing equations to estimate C_c, contributing to estimation of post-yield (i.e. virgin compression) oedometer $\sigma'_v - \varepsilon_a$ charts. It is logical that the aim of such studies has always been finding the least number and the easiest-to-derive input parameters. Table 1 presents several empirical equations proposed for estimation of C_c.

In addition to these equations, Janbu (1963) proposed using constrained modulus, $M = \delta\sigma'_v/\delta\varepsilon_a$, being estimated by [1]:

$$M = m\sigma_a\left(\frac{\sigma'_v}{\sigma_a}\right)^{1-\alpha} \tag{2}$$

which can be used to predict $\sigma'_v - \varepsilon_a$ behavior. The parameters σ_a, σ'_v, m, and α represent the reference stress (100 kPa ≈ 1 atm), effective vertical stress, modulus number, and stress exponent. While the modulus number m reflects the quantity of deformation, the smaller m the larger is the deformation, the stress exponent α reflects the soil type. In general, α = 0.5 represents sands and coarser materials, α = 0 – 0.5 silts, α = 0 non-sensitive clays and α < 0 sensitive clays. For α = 0, the Janbu equation gives and equal stress-strain

* Corresponding author: mohammadsadegh.farhadi@tuni.fi

description as the compression index method. For such non-sensitive clays, Janbu (1998) proposed an estimate for the modulus number equal to [2]:

$$m = \frac{700}{w_n}, \alpha = 0 \tag{3}$$

with a range of ±30% to be used in equation 3, leading to prediction of $\sigma'_v - \varepsilon_a$, only based on natural water content, w_n.

Table 1. Empirical relationships between virgin compression index, C_c, and soil properties.

Equation	Applicability	Ref.
$C_c = 0.85(w_n/100)^{1.5}$	All clays	[3]
$C_c = 0.01(w_n - 5)$	All clays	[4]
$C_c = 0.01w_n$	Clays	[5]
$C_c = 0.01(w_n - 7.549)$	All clays	[6]
$C_c = 0.006(w_L - 9)$	All clays ($w_L < 100\%$)	[4]
$C_c = (w_L - 13)/109$	All clays	[7]
$C_c = 0.54(e_0 - 0.35)$	All clays	[8]
$C_c = 0.4(e_0 - 0.25)$	All clays	[4]
$C_c = 0.156e_0 + 0.0107$	All clays	[9]
$C_c = 0.009w_n + 0.005w_L$	All clays	[5]
$C_c = -0.156 + 0.411e_0 + 0.0058w_L$	All clays	[10]

As mentioned for the equations in Table 1, and similarly for Janbu's equation, it has been always tried to find generalized equations for all clays. But on the other hand, clays may show distinct deformation behaviors. Stress history is a major factor affecting the oedometer deformation behavior. Länsivaara (2019) discussed how flocculation, aging, cementation, structure, and leaching may affect the oedometer $\sigma'_v - \varepsilon_a$ behavior [11]. As an example –which is framed in the scope of the current study also– leaching has led to quite sensitive clays in Scandinavia region [12]. The highly sensitive clays, known as quick clays, led to several large landslides in countries like Norway, Sweden, and Canada, bringing about losses of lives and facilities.

Sensitive soils exist in many regions in Finland, as well. They have been studied at Tampere University, using high-quality samples from several testing sites. It has been of interest to find out how the previously proposed equations can estimate the post-yield $\sigma'_v - \varepsilon_a$ behavior of these sensitive clays. For this purpose, Fig. 2 compares the estimations of equations in Table 1, and also the method by Janbu (1998), with the experimental results, for a CRS oedometer test from Masku testing site.

The estimated $\sigma'_v - \varepsilon_a$ charts, illustrated in Fig. 2 indicate that none of the available C_c-based charts –mentioned in Table 1– could predict the experimental $\sigma'_v - \varepsilon_a$ accurately. Besides, the figure shows also that none of the predictions could model the trend of $\sigma'_v - \varepsilon_a$ for the sensitive clay. Länsivaara (2019) explained that just after the yield point destructuration phase occurs [11]. At this stage, large deformations occur until the deformation curve meets a compression line perhaps parallel to the virgin compression line before leaching (illustrated in [11]). For such behavior, one would need a negative value for α, in order to capture the behavior. For sensitive Finnish clays α values of the order $-1.0, \ldots, -2.0$ are often found [13]. Anyway, this rapid large-strain destrcutration along with the final phase cannot be modelled appropriately by the mentioned empirical correlations –not by the C_c concept in general.

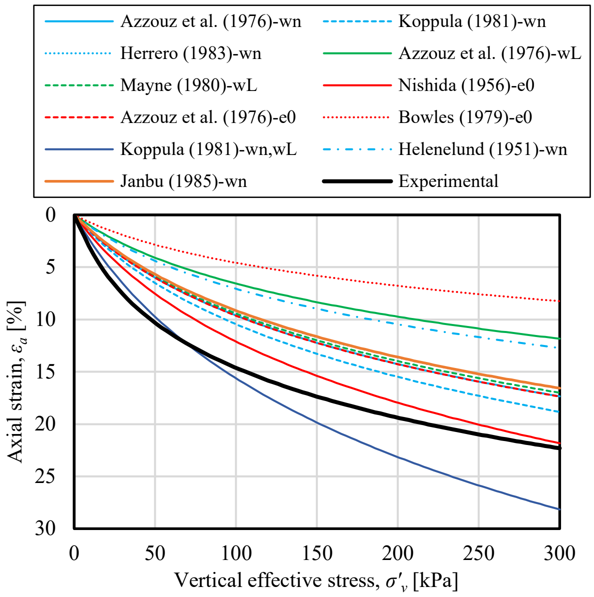

Fig. 2. Comparison of oedometer $\sigma'_v - \varepsilon_a$ charts reconstructed by empirical equations with the experimental measurements, for a sensitive clay specimen from Masku, Finland.

In this regard, Sällfors (1975) proposed a two-phase deformation state after yield point [14]; as depicted in Fig. 3. The two-phase post-yield stages of deformation includes a linear constant value of M_L as the constrained modulus for the destructuration phase. Its corresponding range of σ'_v is called S_L, that equals $\sigma'_L - \sigma'_y$. The slope of post-destructuration phase is linearly variable represented by M', which is the slope of the constrained modulus curve.

Fig. 3 shows the reconstructed $\sigma'_v - \varepsilon_a$ created by the Sällfors parameters: M_0, M_L, M', and S_L, as dotted black line. As can be seen, the reconstructed $\sigma'_v - \varepsilon_a$ fits the experimental measurements accurately. It is evidenced by the figure that the oedometer $\sigma'_v - \varepsilon_a$ of sensitive clays can be modelled accurately using Sällfors parameters.

The scope of this study is prediction of post-yield $\sigma'_v - \varepsilon_a$ using minimal information about soil properties; while the pre-yield prediction is well explored in numerous studies. For this purpose, a novel model is introduced at Tampere University, to predict the post-yield oedometer $\sigma'_v - \varepsilon_a$, for sensitive clays, named PoYOSS$^{Sen}_{\text{Clay}}$, built on Sällfors method.

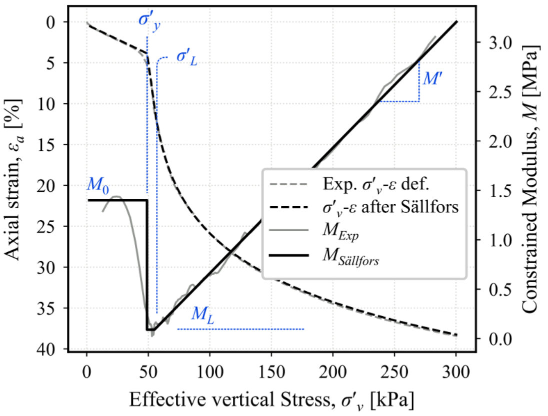

Fig. 3. Sällfors' (1975) parameters for approximating an oedometer $\sigma'_v - \varepsilon_a$ chart: M_0, M_L, M', and $S_L = \sigma'_L - \sigma'_y$ (adapted from [15]).

The aim of the current study has been to assess the correlation between post-yield Sällfors parameters and the soil properties, through submodels of PoYOSS$^{Sen}_{\text{Clay}}$. For this purpose, data from Finnish testing sites were used. And, the results can be employed to improve the predictions of PoYOSS$^{Sen}_{\text{Clay}}$.

2 Database

The utilized database has been the outcome of studies on the Finnish sensitive clays, performed at five different testing sites of FINCONE project, located in the southern region of Finland. The location of the testing sites and their characterization results are described and presented in [15]. The testing sites were named after the closest cities or towns, as: Lempäälä, Masku, Paimio, Perniö, and Sipoo.

The sensitivity, S_t, of the clays at the testing sites were in range [14,122]. The highest S_t was observed at Paimio, and the least values were measured at Masku.

Sensitivity and other experimental soil parameters were measured using high-quality undisturbed samples, taken by φ132 mm TUT tube sampler developed at Tampere University [16]. To study the 1-D deformation behavior of sensitive clays, constant-rate-of-strain (CRS) oedometer tests were performed for samples from depths of 2-9 m, approximately. At Lempäälä, Masku, Paimio, Perniö, and Sipoo, respectively, 14, 7, 22, 40, and 19 oedometer tests were conducted with the strain rate of $\dot{\varepsilon} = 0.4$ % per hour. The normalized distributions of the soil properties are shown in Fig. 4. Details are presented in [15, 16].

2.1 Variation of soil properties

The probabilistic variations of soil properties are depicted in Fig. 4. Each violin plot is derived from a sample set $\{x_i\}_{i=1}^{n}$ where, n=102, by estimating its probability density function using a Gaussian kernel density estimator of the form:

$$\hat{f}(x) = \frac{1}{nh}\sum_{i=0}^{n} K\left(\frac{x - x_i}{h}\right) \tag{4}$$

where, h is the automatically selected bandwidth by different methods such as Scott's Rule ($h = \sigma n^{-1/5}$) or Silverman's Rule ($h = 0.9min(\sigma, IQR/1.34)n^{-1/5}$) [17, 18], n is the number of data points, and $K(u) = \frac{1}{\sqrt{2\pi}} e^{-u^2/2}$ is the Gaussian kernel, in which $u = \frac{x - x_i}{h}$ is a standardized distance between the evaluation point x –at which the estimation of density is desired– and each data point x_i. The parameter σ in Scott's and Silverman's rules is the standard deviation of data, and IQR measures the spread of the middle 50% of data as the difference between first quartile, Q_1, and third quartile, Q_3, of data. The estimated density is normalized between the min and max of data. Within each violin, several statistical descriptors are included: the median is indicated by a horizontal line inside the density, the minimum and maximum values are shown by vertical whiskers, and the mean together with IQR is represented by a colored circular marker and error bar.

The violins corresponding to all parameters of soil properties and Sällfors post-yield parameters are plotted in Fig. 4 enabling a clear comparison of their statistical distributions within a single visual figure. The soil properties are respectively: depths of samples, z, natural water content, w_n, liquid limit, w_L, plastic limit, w_p, sensitivity, S_t, clay fraction, C_f, in-situ vertical effective stress, σ'_{v0}, yield effective stress, σ'_y, and fall cone undrained shear strength at samples' intact state, $S_{u,intact}$. The post-yield Sällfors parameters are: M_L, M', and S_L, as depicted in Fig. 4, on the right.

3 PoYOSS$^{Sen}_{\text{Clay}}$ model

The PoYOSS$^{Sen}_{\text{Clay}}$ model was proposed in [15] as an intelligent model, which predicts the post-yield oedometer stress-strain chart, for sensitive clays, based on minimal information on soil conditions. It consists of five submodels called:

i) data collection: It collects required data from individual files of different experiments.
ii) pre-processing of data: It checks the collected data for the probable problems and tries to refine them, if applicable. As an example, it is shown in [15] how minor flaws in oedometer measurements are refined by approximating via a smoothing method, mathematically. It is noteworthy that for the soil properties which were not measured at the same depths, the information from closest experiments were utilized, being interpolated using piecewise cubic Hermite interpolating polynomial, defined as [19]:

$$\begin{aligned} p(x) = f_i H_1(x) + f_{i+1} H_2(x) \\ + d_i H_3(x) \\ + d_{i+1} H_4(x) \end{aligned} \tag{5}$$

for the subinterval $I_i = [x_i, x_{i+1}]$, where f_i and f_{i+1} are the observed values at x_i and x_{i+1}, and:

$$d_j = p'(x_j), j = i, i+1,$$

and the $H_k(x)$ are the Hermite basis functions for the interval, as:

$$H_1(x) = \varphi\left(\frac{x_{i+1}-x}{h}\right) = \varphi(1-t)$$

$$H_2(x) = \varphi\left(\frac{x-x_i}{h}\right) = \varphi(t)$$

$$H_3(x) = -h\psi\left(\frac{x_{i+1}-x}{h}\right) = -h\psi(1-t)$$

$$H_4(x) = h\psi\left(\frac{x-x_i}{h}\right) = h\psi(t)$$

where, $h = x_{i+1} - x_i$, $t = \frac{x-x_i}{h}$, $\varphi(t) = 3t^2 - 2t^3$, and $\psi(t) = t^3 - t^2$.

iii) determination of moduli: An evolutionary optimization model was developed specifically for finding Sällfors parameters: M_0, M_L, M', and S_L, for all oedometer measurements. Two objective functions were devised in multi-objective non-dominated sorting genetic algorithm II (NSGA-II) model to find the optimum parameters, fitting the reconstructed $\sigma'_v - \varepsilon_a$ to the lab measurements. Among the Pareto front optimal solutions (as the output of NSGA-II model), one was selected as the optimum solution by finding the equilibrium point between the objectives, through a Game theory bargaining method, called Borda scoring, as a social-choice rule (SCR) method. Meanwhile, it is presented in [15] that all pareto front solutions reconstructed the experimental $\sigma'_v - \varepsilon_a$ accurately.

iv) learning-based predictor: This submodel approximates the post-yield Sällfors parameters using soil properties. For this purpose, a multi-layer perceptron (MLP) artificial neural network (NN) was modelled [15], using 10 perceptrons, and dividing database to fixed divisions of train, test and validation. To train the model, three different optimization methods were utilized: (a) scaled-conjugate gradient (SCG), (b) Levenberg-Marquardt (LM), and (c) Bayesian regularization (BR) –explained mathematically in [15, 20, 21]. The accuracy of NN predictions were evaluated based on several error criteria: root mean squared error (*RMSE*), Pearson correlation coefficient (*R*), average bias, and supremum norm (known also as Chebyshev distance). There was the shortage of evaluating the dependency of each post-yield Sällfors parameter upon various soil properties in [15], which is conducted in this study.

v) conflict-resolution model(s): One of the advantageous aspects of artificial intelligence (AI) models is how randomly their intelligence may respond in different cases. They usually result into optimal solutions, that may vary if their training process is repeated –specifically for supervised learning models. This may emanate from the optimization methods in training. Although this can be an advantage in so many cases, herein, the possibility to compare NNs for different soil properties restricts the solution to be a unique model. Hence, the NN models –repeatedly trained by the three optimization methods (SCG, LM, and BR)– were reassessed to find one suitable representative of them, through the Game theory, conflict-resolution models: Borda scoring [22] and Condorcet's choice method [22]; which are both renowned as social choice rule (SCR) methods. Details are explained in [15].

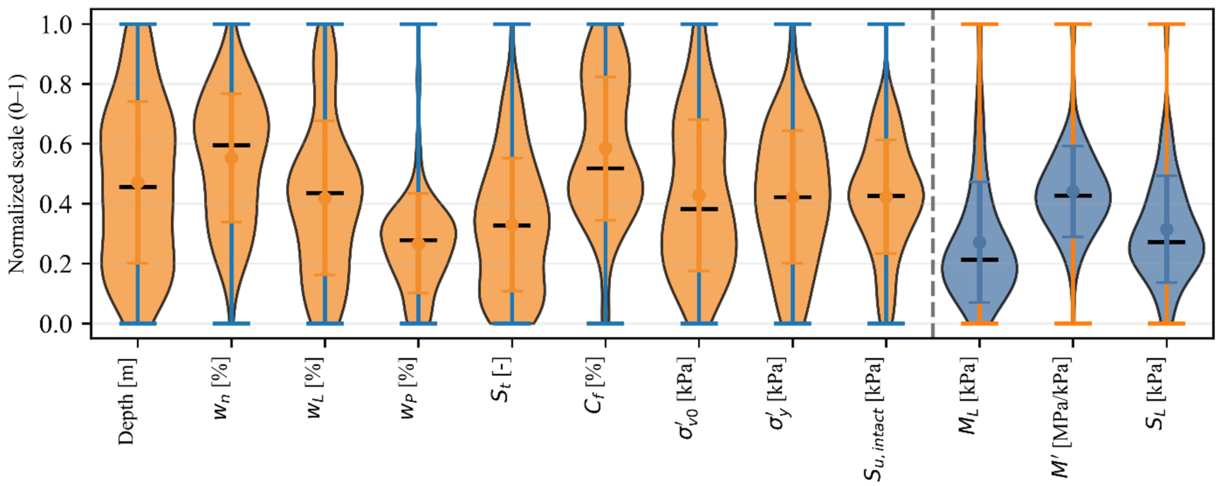

Min	2.04	55.90	40.09	23.00	14.42	36.04	19.16	13.41	6.92	61.40	9.74	2.31
Median	5.10	98.30	64.00	29.11	49.69	68.11	32.45	39.34	14.60	132.47	12.83	9.54
Mean	5.20	95.28	63.09	28.87	49.90	72.19	34.07	39.39	14.56	151.79	12.93	10.67
St. dev	1.81	15.27	14.13	3.68	23.94	14.84	8.81	13.61	3.42	67.38	1.10	4.75
Max	8.75	127.20	95.00	45.00	122.01	97.95	54.00	74.93	24.98	395.48	16.98	28.90

Fig. 4. Variation of soil properties and their statistical estimators.

4 Optimization methods in NN

The three optimization methods SCG, LM, and BR were used to train NNs, in order to assess their impact on the results. Training was repeated for 1000 times, providing 1000 trained networks, to predict each of M_L, M', and S_L, using soil properties as input variables either individually or in combinations, as mentioned in Tables 3(a-c) and Figs. 6-8.

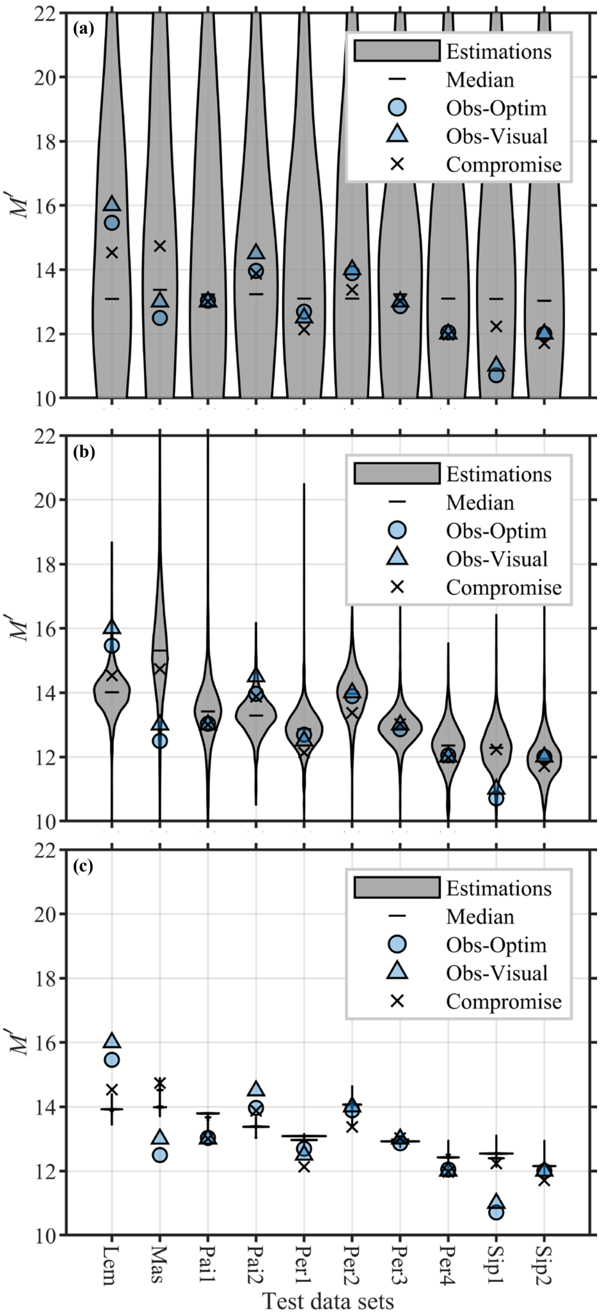

Fig. 5. Variations of M' predicted repeatedly using NN, based on w_n and S_t, for the three optimization methods: a) SCG, b) LM, and c) BR. The results are depicted for test data division.

In order to illustrate the impact of the optimization methods on the predicted Sällfors parameters, violin plots were fitted to the outputs of 1000 NNs to predict M', for test data division, as depicted in Figs. 5(a-c). As can be observed, the results of SCG optimization method were the most variable, and the least variable results were observed for BR. It shows that if SCG is used for training, the predicted M' can be significantly over- or under-estimated, which consequently leads to risks or non-economical designs in practice.

The median of NN predictions for SCG were almost equal for all test data sets (Fig. 5(a)), while they were more variable for LM and BR (Figs. 5(b-c)). It shows that SCG leads to overly generalized results. On the other hand, pairwise comparison of the results in Figs. 5(b) and (c) shows almost equal medians for the same test data sets, using both LM and BR. These figures highlight the significance of the training optimization method to predict deformation behavior.

Figs. 5(a-c) show also the Sällfors parameters fitted visually by an engineer (Obs-Visual), compared with the results of the third submodel, as the optimized parameters fitted by the developed multi-objective model (Obs-Optim). These values can be compared with the compromise, derived from the fifth submodel, i.e. conflict-resolution models. The compromise was the result of the selected NN among the 1000 trained ones, which is regarded as the output of $\text{PoYOSS}_{\text{Clay}}^{Sen}$. It can be seen that for most of the test data sets, compromise has been close to the Obs-Optim parameters, which implies that the predictions of $\text{PoYOSS}_{\text{Clay}}^{Sen}$ have been in good agreement with the experimental measurements.

5 Correlated soil properties

Pairwise Pearson correlation among individual soil properties and the post-yield Sällfors parameters is studied in [15]. M_L was best correlated with w_n ($R = -0.70$). M' was best correlated with w_L ($R = -0.67$). And, there was no good correlation between S_L and any of soil properties. Here, the focus is on the correlations between the $\text{PoYOSS}_{\text{Clay}}^{Sen}$-predicted post-yield Sällfors parameters and soil properties. For this purpose, a correlation analysis was performed, for individual soil properties, and the results are presented in Tables 3(a-c) for M_L, M', and S_L, respectively. The performance criteria in the Tables are root mean squared error ($RMSE$), Pearson correlation coefficient (R), average of bias ($bias_{avg}$), and supremum norm (known also as Chebyshev distance).

The heatmaps in Table 2(a) are created by the performance criteria comparing the NN predictions with experimental M_L. It shows that M_L was mostly correlated with w_n. Almost all performance criteria approve it. Besides, M_L is also well correlated with z and $S_{u,intact}$. The calculated supremum norm ranks w_p as the second most correlated parameter. Based on such reasoning, four combinations of soil properties were studied, as presented in Fig. 6, for prediction of M_L.

Similar analysis was performed for M'. Table 3(b) shows that M' was best correlated with w_n, as well. Strong correlations can be observed for the other two properties, w_L and $S_{u,intact}$, also. The calculated performance criteria show comparable values for the three properties. Hence, their combinations were also studied, as shown in Fig. 7.

Table 2. Performance criteria for pairwise correlations between soil properties and Sällfors parameters: (a) M_L, (b) M', and (c) S_L.

(a)

M_L	z	w_n	w_L	w_p	S_t	C_f	σ'_{v0}	σ'_y	$S_{u,int}$
RMSE	41.6	35.0	45.7	47.0	47.3	48.9	48.5	52.2	42.2
R	0.75	0.83	0.68	0.67	0.65	0.62	0.63	0.55	0.74
$bias_{avg}$	1.05	1.01	1.00	1.00	0.99	1.01	1.00	1.03	0.98
Sup. norm	158	140	174	143	183	258	149	166	176

(b)

M'	z	w_n	w_L	w_p	S_t	C_f	σ'_{v0}	σ'_y	$S_{u,int}$
RMSE	1.12	0.90	0.93	1.04	1.14	1.06	1.08	1.11	0.92
R	0.55	0.75	0.73	0.63	0.53	0.61	0.60	0.56	0.73
$bias_{avg}$	1.00	1.00	1.01	1.00	1.00	1.00	1.01	1.00	1.00
Sup. norm	3.59	2.37	2.74	3.09	3.60	2.90	3.59	4.45	4.27

(c)

S_L	z	w_n	w_L	w_p	S_t	C_f	σ'_{v0}	σ'_y	$S_{u,int}$
RMSE	3.42	3.80	3.61	3.29	3.69	3.70	3.71	3.23	3.72
R	0.58	0.43	0.52	0.63	0.48	0.48	0.48	0.64	0.47
$bias_{avg}$	1.00	1.02	1.01	0.99	1.02	1.01	1.04	1.02	0.99
Sup. norm	11.1	18.3	13.2	10.4	13.6	13.8	11.5	9.7	13.4

Similar PoYOSS$^{Sen}_{\text{Clay}}$-based correlations were studied for S_L, as presented in Table 3(c). Comparison of R values with Tables 3(a-b) proves that S_L was not similarly well correlated with the soil properties, individually. Nevertheless, the strongest correlation can be observed for σ'_y, w_p, and z, individually; and, Fig. 8 shows similar results for their combinations.

Figs. 6(a-d) illustrate distribution of estimated versus observed M_L based on the four combinations of soil properties presented in the heatmap underneath. The linear regression dotted lines illustrate if M_L is under- or over-estimated. The performance criteria of the heatmap prove that the best correlation was observed for $[w_n, S_{u,int}]$. Table 3(a) showed that M' was best correlated with w_n, as a single input variable. But considering the combination of $[w_n, S_{u,int}]$ improved R from 0.83 to 0.91. The heatmap shows including z as one additional parameter did not improve the performance criteria.

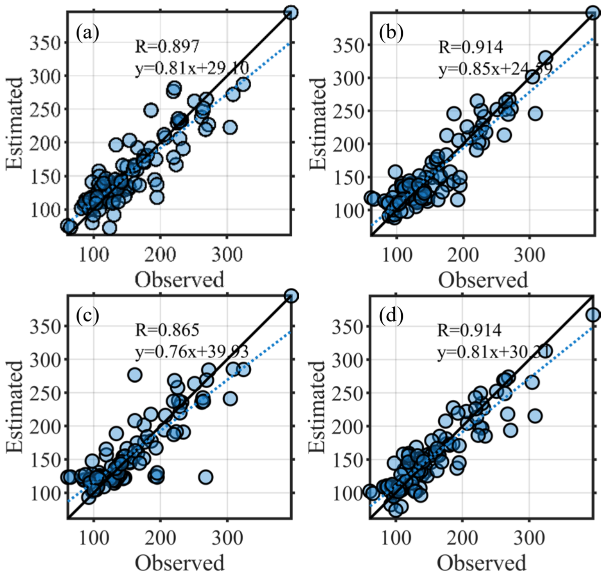

	(a)	(b)	(c)	(d)
M_L	$[z, w_n]$	$[w_n, S_{u,int}]$	$[w_n, w_p]$	$[z, w_n, S_{u,int}]$
RMSE	27.7	25.3	31.5	25.4
R	0.90	0.91	0.86	0.91
$bias_{avg}$	1.01	1.00	0.98	1.00
Sup. norm	81.8	76.1	144.3	93.4

Fig. 6. Charts atop illustrate the estimated versus the experimental M_L. Estimated values are based on NN for four soil parameters combinations presented in the heatmap underneath; presented along with other performance criteria.

Figs. 7(a-d) illustrate observed-estimated M' distributions along with linear regression line and R values, for the combinations of soil properties presented on the heatmap. They show that the post-destructration phase has been correlated with more soil properties: $[w_n, w_L, w_p, S_{u,int}]$, while the constrained modulus at destructation phase was the best correlated with $[w_n, S_{u,int}]$. The performance criteria in Fig. 7 show that excluding w_p from $[w_n, w_L, w_p, S_{u,int}]$ did not degrade the estimations considerably. Such observation may lead to reducing the experimental workload, by skipping plasticity index test, in projects; provided that PoYOSS$^{Sen}_{\text{Clay}}$ is applied to predict the $\sigma'_v - \varepsilon_a$ behavior. Furthermore, comparing the heatmap with Table 3(b) proved improvement of R from 0.75 (for w_n) to 0.94 (for $[w_n, w_L, w_p, S_{u,int}]$).

Among the three Sällfors parameters, S_L was predicted the least accurately based on individual soil properties, as presented in Table 3(c). The highest R was observed for σ'_y; but using the combination of $[\sigma'_y, w_L, z]$ improved R from 0.64 to 0.83, and *RMSE* from 3.23 to 2.37; although, the supremum norm was increased (Fig. 8). It is interesting how including depth of samples, z, improved the predictions, which may not be regarded as a real geotechnical property.

https://doi.org/10.1051/e3sconf/202673003002

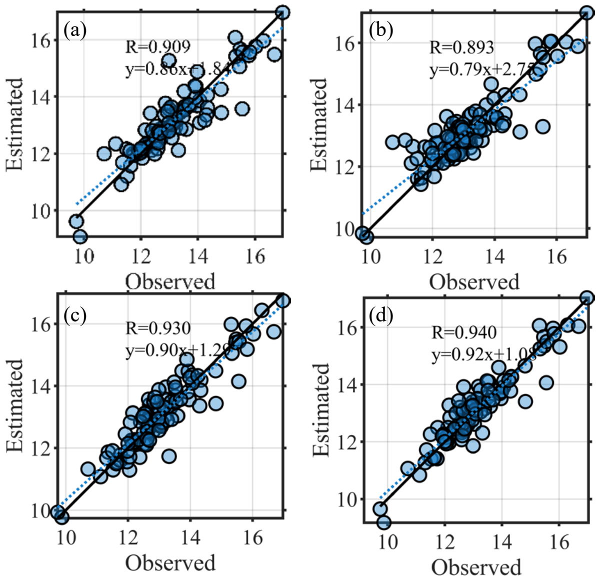

M'	(a) $[w_n, w_L]$	(b) $[w_n, S_{u,int}]$	(c) $[w_n, w_L, S_{u,int}]$	(d) $[w_n, w_L, w_p, S_{u,int}]$
RMSE	0.56	0.60	0.50	0.46
R	0.91	0.89	0.93	0.94
$bias_{avg}$	1.00	1.00	1.00	1.00
Sup. norm	2.28	2.27	1.59	1.50

Fig. 7. Charts atop illustrate the estimated versus the experimental M'. Estimated values are based on NN for four soil parameters combinations presented in the heatmap underneath; presented along with other performance criteria.

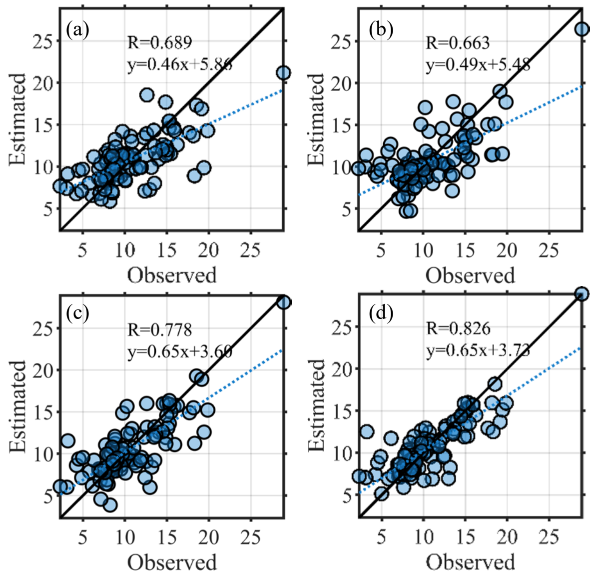

S_L	(a) $[\sigma'_y, w_p]$	(b) $[\sigma'_y, z]$	(c) $[\sigma'_y, w_L]$	(d) $[\sigma'_y, w_L, z]$
RMSE	3.05	3.16	2.66	2.37
R	0.69	0.66	0.78	0.83
$bias_{avg}$	1.00	1.02	1.03	1.00
Sup. norm	9.59	8.16	8.32	9.30

Fig. 8. Charts atop illustrate the estimated versus the experimental S_L. Estimated values are based on NN for four soil parameters combinations presented in the heatmap underneath; presented along with other performance criteria.

It is noteworthy that the pairwise Pearson correlation [15] resulted into $R = -0.17$ (for w_L) as the strongest correlation found between S_L and soil properties. However, Table 3(c) shows that for w_L-based predicted versus compared S_L: $R = 0.52$; even though, a low pairwise correlation was reported between them.

The average of bias being close to 1 implies that the equilibrium NN chosen by Borda scoring was selected correctly. Besides, a low supremum norm reflects the capability of the chosen NN to capture the variability of the predicted parameters.

6 Validation of predictions

It is worthwhile to evaluate the impact of the identified highly correlated parameters on the $\sigma'_v - \varepsilon_a$ charts. For this purpose, Figs. 9(a-b) compare two typical oedometer measurements with PoYOSS$^{Sen}_{\text{Clay}}$ predictions reconstructed from the estimations of M_L, M', and S_L. They are compared with the predictions of the aforementioned empirical equations. It can be seen that PoYOSS$^{Sen}_{\text{Clay}}$ have predicted the typical trend of $\sigma'_v - \varepsilon_a$ for sensitive clays, much better than the other methods. Further, PoYOSS$^{Sen}_{\text{Clay}}$ is able to predict the $\sigma'_v - \varepsilon_a$ behavior very accurately, as shown in Fig. 9(b).

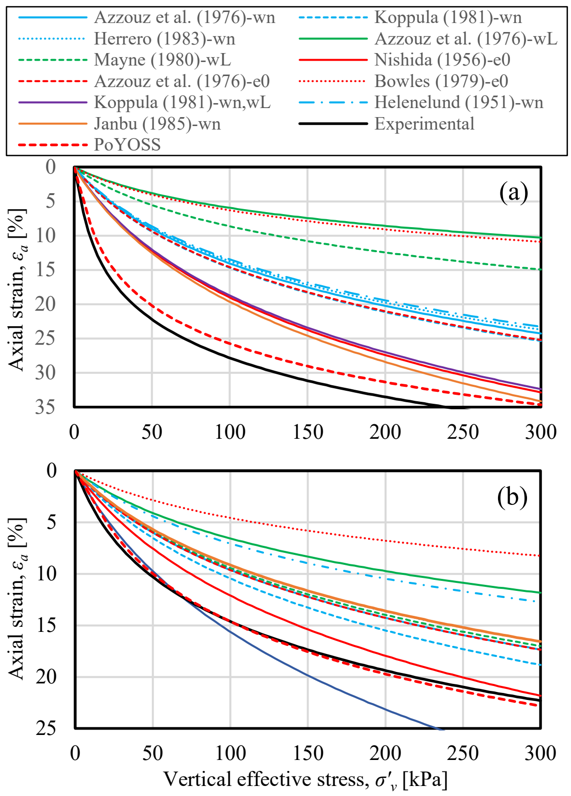

Fig. 9. Comparison of PoYOSS$^{\text{Sen}}_{\text{Clay}}$predictions with empirical equations, for typical tests from: a) Sipoo, and b) Masku.

7 Conclusions

A novel model, $\text{PoYOSS}_{\text{Clay}}^{Sen}$, was proposed to predict the behavior of vertical effective stress, σ'_v–axial strain, ε_a, for constant-rate-of-strain (CRS) oedometer tests in Finnish sensitive clays. In one of its five submodels, a supervised learning model, MLP neural network (NN) has been utilized to estimate the three Sällfors post-yield parameters: M_L, M', and S_L. The most accurate trained NNs were sought in this study to find the soil properties best correlated with every Sällfors post-yield parameter. This correlative study showed that three Sällfors parameters M_L, M', and S_L were best correlated with w_n, w_n, and σ'_y, respectively, as individual parameters. Among the available data, the best combinations of soil properties correlated with M_L, M', and S_L have been $[w_n, S_{u,int}]$, $[w_n, w_L, w_p, S_{u,int}]$, and $[\sigma'_y, w_L, z]$, respectively. The findings also indicated that:

1) The optimization model, used for training the NN, can lead to variable estimations of target parameters. So, it is necessary to validate the obtained results. For this purpose, in the current study a Game theory, social choice rule, Borda scoring method was used to find the equilibrium point, considering several performance criteria.
2) $\text{PoYOSS}_{\text{Clay}}^{Sen}$ is capable to predict the $\sigma'_v - \varepsilon_a$ curves accurately.

It should be noted that there are other influential factors –such as regularization method in the NN, or other learning models– that can affect accuracy and regularization of estimations of the target parameters. They may affect the correlative study results; although, this study has tried to find generalized findings through considering multi-criteria decision making, conflict-resolution models, and repetitions of training models.

Väylävirasto is acknowledged for their financial support for projects FINCONE I & II. Tekniikan Edistämissätiö (Finnish Foundation for Technology Promotion) is acknowledged for grant no. JNR 8375, for the corresponding author. Bruno Di'Buo and Juha Selänpää are acknowledged for their great support by conducting experimental measurements.

References

1. N. Janbu, Soil compressibility as determined by oedometer and triaxial tests: Proceedings of the 2nd European Conference on Soil Mechanics and Foundation Engineering, Wiesbaden, Germany, 1: 19—25 (1963).
2. N. Janbu, Sediment deformations: A classical approach to stress-strain-time behaviour of granular media as developed at NTH over a 50 year period, Department of Geotechnical Engineering NTNU/NTH, Trondheim, Bulletin, 35 (1998).
3. Helenelund, K.V. (1951). Om konsolidering och sättning av belastade marklager, Maa- ja vesiteknillisiä tutkimuksia 6, Helsinki.
4. A.S. Azzouz, R.J. Krizek, R.B. Corotis, Regression analysis of soil compressibility, J. Soils Found., 16(2): 19–29 (1976). https://doi.org/10.3208/sandf1972.16.2_19
5. S.D. Koppula, Statistical estimation of compression index, Geotechnical Testing Journal, 4(2): 68–73 (1981).
6. O. Rendon-Herrero, Closure to "universal compression index equation", J. Geot. Eng., 109(5): 755—761 (1983).
7. P.W. Mayne, Cam-clay predictions of undrained strength, J. Geot. Eng. Division, 106(11): 1219—1242 (1980). https://doi.org/10.1061/AJGEB6.0001060
8. Y. Nishida, A brief note on compression index of soil, Journal of the Soil Mech. Found. Division, 82(3): 1027–1 (1956). https://doi.org/10.1061/JSFEAQ.0000015
9. J.E. Bowles, Physical and geotechnical properties of soils, McGraw-Hill Book Company, New York, USA (1981).
10. A.W.N. Al-Khafaji, O.B. Andersland, Equations for compression index approximation, J. Geotech. Eng., 118(1): 148–153 (1992). https://doi.org/10.1061/(ASCE)0733-9410(1992)118:1(148)
11. T.T. Länsivaara, Determination of creep properties of clays from VRS oedometer tests, Geotech. Geol. Eng., 38(2): 1857—1871 (2019). https://doi.org/10.1007/s10706-019-01135-1
12. I.TH. Rosenqvist, Marine clays and quick clay slides in south and central Norway. Norges Geologiske UndersØkelse, No. 212q., Oslo (1960).
13. T.T. Länsivaara, Painumalaskentamenetelmien käyttökelpoisuuden arviointi, Tielaitoksen selvityksiä (2000).
14. G. Sällfors, Preconsolidation pressure of soft, high-plastic clays, Doctoral dissertation, Chalmers University of technology, Gothenburg, Sweden (1975).
15. M.S. Farhadi, T.T. Länsivaara, $\text{PoYOSS}_{\text{Clay}}^{Sen}$: A novel model for post-yield oedometer stress-strain prediction of sensitive clays.
16. B. Di Buò, J. Selänpää, T.T. Länsivaara, M. D'Ignazio, Evaluation of sample quality from different sampling methods in Finnish soft sensitive clays. Canadian Geotech. J., 56(8), 1154—1168 (2019). https://doi.org/10.1139/cgj-2018-0066
17. D.W. Scott, Multivariate density estimation: Theory, practice, and visualization, John Wiley & Sons, Inc. (1992). https://doi.org/10.1002/9780470316849
18. B.W. Silverman, Density estimation for statistics and data analysis, Chapman & Hall (1998).
19. F.N. Fritsch, R.E. Carlson, Monotone piecewise cubic interpolation, SIAM J. Numer. Anal. **17**, 2 (1980). https://doi.org/10.1137/0717021
20. T.T. Länsivaara, M.S. Farhadi, P. Samui, Performance of traditional and machine learning-based transformation models for undrained shear strength. Arab. J. Geosci. 16(3), 183 (2023). https://doi.org/10.1007/s12517-022-11173-4
21. G. Habibagahi, A. Bamdad, A neural network framework for mechanical behavior of unsaturated soils. J. Geot. Eng. 40, 684—693 (2003). https://doi.org/10.1139/t03-004
22. M. Sheikhmohammady, K. Madani, Bargaining over the Caspian Sea—the largest lake on the earth, World Environmental and Water Resources Congress 2008: Ahupua'A, 1–9 (2008). https://doi.org/10.1061/40976(316)262